ISPRS Journal of Photogrammetry and Remote Sensing 165 (2020) 133–139

Contents lists available at ScienceDirect

ISPRS Journal of Photogrammetry and Remote Sensing

journal homepage: www.elsevier.com/locate/isprsjprs

An automated PCA-based approach towards optimization of the rational function model

Saeid Gholinejad[a], Alireza Amiri-Simkooei[a,*], Sayyed Hamed Alizadeh Moghaddam[b], Amin Alizadeh Naeini[c]

[a] Department of Geomatics Engineering, Faculty of Civil Engineering and Transportation, University of Isfahan, Isfahan 8174673441, Iran
[b] Faculty of Geodesy and Geomatics Engineering, K. N. Toosi University of Technology, Tehran 1996715433, Iran
[c] Department of Earth and Space Science and Engineering, York University, 4700 Keele St, Toronto, ON M3J1P3, Canada

ARTICLE INFO

Keywords:
Rational function model
Principal component analysis
Noise reduction
Thresholding ridge ratio

ABSTRACT

The existence of several unnecessary and highly correlated coefficients in the rational function model (RFM), known as rational polynomial coefficients (RPCs), leads to an ill-posed design matrix. Under such a condition, any small perturbation, including errors in the problem's input, causes drastic changes in the final results. The ill-posedness of the design matrix, intrinsic to the RFM problem, can be amplified due to the errors in the ground and image coordinates of the control points. The principal component analysis (PCA)-based RFM optimization method has already been applied to reduce the impact of ill-posedness of the design matrix. Despite its efficacy, the existence of a case-sensitive tunable threshold value in this method has overshadowed its efficiency. To address this problem, we propose an automated PCA-based RFM optimization, called APCA-RFM method, which is based on the thresholding ridge ratio criterion. In APCA-RFM, the data itself is used to obtain the threshold value and hence to separate the noise from the signal. Experiments conducted on different data sets demonstrated the high performance of the proposed method to come up with a solution to the challenge of an appropriate threshold value. Additionally, the experimental results proved the superiority of the proposed APCA-RFM in comparison with recently published methods dealing with the ill-posedness problem of RFM.

1. Introduction

To achieve an image free from any geometric distortions, known as an ortho-image, researchers use geometric correction as one of the basic and essential steps of satellite image processing. This process provides the preliminaries for subsequent satellite image processing such as change detection, the fusion of multi-source data, generating digital elevation models (DEMs), image classification, and several other processes (Toutin, 2004). Among the various geometric correction models, the rational function model (RFM) has been widely considered by researchers and vendors of satellite images due to a couple of reasons. For example, they are independent of the sensor type, flexible in the coordinate systems, and keep the sensor information confidential (Tao and Hu, 2001).

The RFM is a mathematical model composed of the ratio of two polynomials, usually of third-order. Despite the many advantages of this model, the existence of a large number of highly correlated parameters, known as rational polynomial coefficients (RPCs), in this model leads to two destructive ill-posedness and overparameterization phenomena (Alizadeh Moghaddam et al., 2018b). As a result of these two phenomena, the design matrix of the RFM problem becomes ill-posed. Under such circumstances, the existence of a small level of noise or errors in input data dramatically affects the final results. On the other hand, the ill-posedness of the design matrix abnormally enlarges the RPCs in the procedure of the RFM optimization. To address these problems, researchers have proposed several methods in the literature in the form of regularization-based techniques.

The ℓ_2-norm regularization-based methods are among the first groups of regularization-based techniques that handle the problem (Yuan and Lin, 2008; Zhou et al., 2012; Wu and Ming, 2016; Cao and Fu, 2018). The main focus of these methods is on the ill-posedness phenomenon. In these methods, RPCs are determined via minimizing the summation of ℓ_2-norm of the residuals and ℓ_2-norm of the RPCs. Imposing ℓ_1-norm of RPCs to the main problem of the RFM is another regularization-based technique for RFM optimization (Long et al., 2015). The ℓ_1-norm minimization approximately yields a sparse solution. Accordingly, a number of unnecessary RPCs are removed from the RFM structure, and therefore, the effects of the overparameterization

* Corresponding author.
E-mail address: amiri@eng.ui.ac.ir (A. Amiri-Simkooei).

https://doi.org/10.1016/j.isprsjprs.2020.05.011
Received 23 March 2020; Received in revised form 13 May 2020; Accepted 13 May 2020
Available online 30 May 2020

phenomenon are resolved or reduced.

As previously mentioned, there exist a lot of unnecessary parameters in the RFM structure that should be removed to reduce the overparameterization effect. In this regard, providing a sparse solution, ℓ_0-norm regularization can eliminate these additional RPCs. Since the direct ℓ_0-norm minimization is a non-convex and NP-hard problem, this task is performed using an indirect manner in the form of computational variable selection methods (Alizadeh Moghaddam et al., 2018b; Zhang et al., 2012; Tengfei et al., 2014; Moghaddam et al., 2017; Naeini et al., 2020) and meta-heuristic methods (Valadan Zoej et al., 2007; Alizadeh Naeini et al., 2017; Jannati et al., 2017; Alizadeh Moghaddam et al., 2018a; Gholinejad et al., 2019a; Gholinejad et al., 2019b; Gholinejad et al., 2020). To identify the optimum RPCs, variable selection methods usually use a mathematical procedure based on some of the RFM concepts, while meta-heuristic methods consciously search the solution space based on a cost function, which is usually the root mean squares error (RMSE) over some ground control points (GCPs), called dependent check points (DCPs).

In the case of an ill-posed problem, any small perturbations in the inputs may lead to dramatic changes in the final results (Öztürk and Akdeniz, 2000). The inputs of the RFM problem are image and ground coordinates of the GCPs, in which the existence of errors and noise is inevitable. Since these errors are directly transmitted to the design matrix of RFM, the estimation of RPCs encounters serious problems. To address these problems, a principal component analysis (PCA)-based method, namely PCA-RFM (Naeini et al., 2020), has recently been proposed, which successfully improves RPCs determination. This method, which can be considered as a variable selection method, tries to diminish the impacts of ill-posedness and overparameterization phenomena by the noise reduction in the design matrix. In the PCA-RFM, first, the PCA transformation is performed on the columns of the design matrix. Therefore, 78 principal components (PCs), which equals the number of RPCs, are generated in the PC space. Among these PCs, those with eigenvalues less than a pre-defined threshold value are excluded. After that, by applying the inverse PCA transformation on the remained PCs, the noise reduced design matrix is obtained. Finally, owing to the rank deficiency of the new design matrix, the QR decomposition with column pivoting along with the least-squares method (Golub and Van Loan, 2012) is used to estimate RPCs.

Despite the high performance of the PCA-RFM in determining accurate solutions of the RFM optimization, it is a challenging task to choose a proper threshold value to omit the noise-related PCs and keep the signal-related ones. To tackle this problem, inspired by Zhu et al. (2019), this study proposes an automatic method based on the thresholding ridge ratio criterion to specify the number of signal-related PCs during the PCA-RFM procedure. In the first step of this method, called automated PCA-RFM (APCA-RFM), the eigenvalues of the sample correlation and sample covariance matrices of the design matrix are obtained. The differences between the corresponding eigenvalues, hereafter named “eigendiffs” for convenience, are then calculated in the next step. Theoretically, the eigendiffs, corresponding to the noise-related PCs, should be equal to zero (Chang and Du, 2004). In other words, the number of noise-related PCs is equal to the number of PCs whose corresponding eigendiffs are equal to zeros. In practice, the eigendiffs are never equal to zero. But the ratios of the consecutive eigendiffs are very close to one. When a non-normalized design matrix is used, high-value eigendiffs are produced. However, the ratios of the consecutive eigendiffs corresponding to the noise-related PCs are exactly equal to one. Accordingly, in the proposed method, the ratios of the consecutive eigendiffs are determined. The number of values that differ from one ($\neq 1$) is equal to the number of signal-related PCs that should remain in the PCA-RFM procedure.

The remainder of this study is organized as follows. The methodology of the APCA-RFM and the procedure for determining the number of signal-related PCs, based on the thresholding ridge ratio criterion, are introduced in Section 2. Section 3 describes the experimental results on different data sets. Finally, we conclude this study in Section 4.

2. Methodology

2.1. PCA-based RFM optimization

The RFM is composed of two equations in the form of Eqs. (1) and (2), which transform the coordinates in the ground space to the coordinates in the image space, and vice versa.

$$r = \frac{P_1(X, Y, Z)}{P_2(X, Y, Z)} \tag{1}$$

$$c = \frac{P_3(X, Y, Z)}{P_4(X, Y, Z)} \tag{2}$$

where r and c are the normalized image coordinates, and X, Y, and Z are the normalized ground coordinates. Moreover, P_i $(i = 1, \cdots, 4)$ are polynomials, usually of order three. After linearizing the above equations and participation of GCPs, the following equation is formed:

$$l = Ax + e \tag{3}$$

where $l_{2n\times1}$, $A_{2n\times78}$, $x_{78\times1}$, and $e_{2n\times1}$ are the observations vector, design matrix, unknowns vector, and residuals vector, respectively. Furthermore, n is the number of GCPs, and 78 is the number RPCs. To find the unknown RPCs, the first strategy is to apply the ordinary least-squares as follows:

$$x = (A^TA)^{-1}A^Tl \tag{4}$$

Observations are always subject to measurement noise. These errors are inevitably transmitted to the design matrix and observation vector. Therefore, the design matrix is always subject to noise. The noise-free design matrix $\widehat{A}$ can be calculated as follows:

$$\widehat{A} = A + \widehat{E} \tag{5}$$

where $\widehat{E}_{2n\times78}$ is the estimated error matrix. The matrix $\widehat{E}$ contains information that makes the nearly rank-deficient (i.e. ill-posed) matrix A to a strictly rank-deficient matrix $\widehat{A}$.

To obtain (or realistically approximate) $\widehat{A}$, PCA-RFM was introduced in Naeini et al. (2020). In PCA-RFM, first, the mean-centered design matrix $\widetilde{A}$ is calculated to facilitate further calculations.

$$\widetilde{A} = A - \text{mean}(A) \tag{6}$$

where $\text{mean}(A)_{2n\times78}$ is a matrix for which each individual column has identical entries equal to the mean value of the corresponding column in A. After specifying $\widetilde{A}$, the covariance matrix $C = \widetilde{A}^T\widetilde{A}/(2n)$ of $\widetilde{A}$ is determined. Then, the PCA transformation is applied to as follows:

$$Q = \widetilde{A}V \tag{7}$$

where V is the matrix of eigenvectors of C, and Q is a matrix containing 78 PCs, equals to the number of RPCs. If $\lambda_1, \cdots, \lambda_{78}$ are the decreasingly ordered eigenvalues of C, the number P of the signal-related PCs is calculated as:

$$P = \max_j \left\{ j: \lambda_j > t \right\}, j = 1, \cdots, 78 \tag{8}$$

where t is a user-defined threshold value, determined in a trial and error manner. After determining P, the matrix of eigenvectors is decomposed into two matrices $V_1 = [v_1, \cdots, v_P]$ and $V_2 = [v_{P+1}, \cdots, v_{78}]$, respectively corresponding to the signal-related and noise-related PCs.

Once the V_1 is assigned, the $\widehat{A}$ is determined through the inverse PCA transformation and the inverse mean-centering process as follows:

$$\widehat{A} = \widetilde{A}V_1V_1^T + \text{mean}(A) \tag{9}$$

Finally, the RPCs are estimated by the QR decomposition with column pivoting and the least-squares method (Golub and Van Loan, 2012).

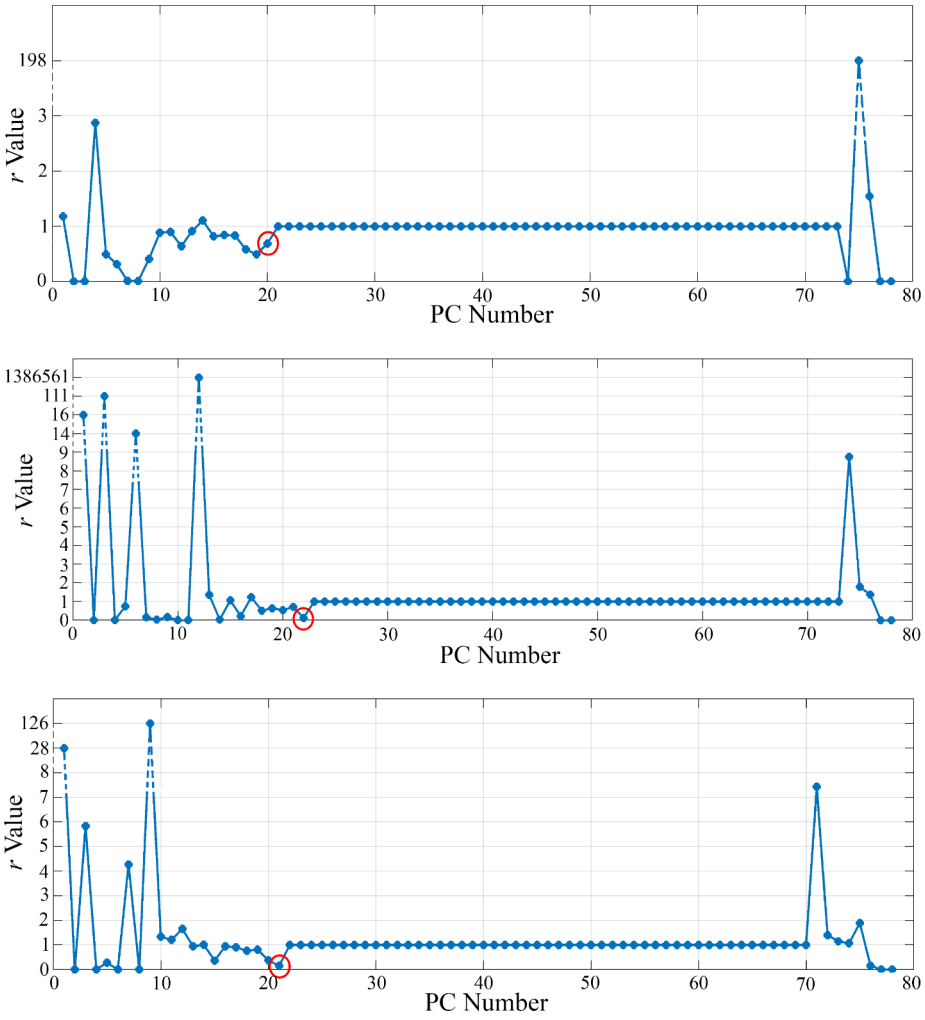

Fig. 1. Graph of the r values for three sample data sets, in which the PC corresponding to P value has been specified by circle.

2.2. Signal-related PCs determination

If each of the rows and each of the columns of the design matrix A are respectively considered as a sample and a property, the sample correlation ($\widehat{R}_A$) and the sample covariance ($\widehat{\Sigma}_A$) matrix of A are determined as follows:

$$\widehat{R}_A = \frac{1}{2n}\sum_{i=1}^{2n} A_i^T A_i \tag{10}$$

and

$$\widehat{\Sigma}_A = \frac{1}{2n}\sum_{i=1}^{2n} (A_i - \overline{A})^T \left(A_i - \overline{A}\right) \tag{11}$$

where A_i is the ith row of A and $\overline{A} = \frac{1}{2n}\sum_{i=1}^{2n} A_i$.

Comparing Eqs. (10) and (11), the following equation can be inferred:

$$\widehat{R}_A = \widehat{\Sigma}_A + \overline{A}^T\overline{A} \tag{12}$$

Suppose that $\mu_1, \cdots, \mu_{78}$ and $\sigma_1, \cdots, \sigma_{78}$ are the ordered eigenvalues of the sample correlation and sample covariance matrix of A, respectively. It is expected that these eigenvalues satisfy the following properties (Chang and Du, 2004):

$$\begin{cases} s_i = \mu_i - \sigma_i > 0, & \text{in the case of signal.} \\ s_i = \mu_i - \sigma_i = 0, & \text{in the case of noise.} \end{cases} \tag{13}$$

Eq. (13) can also be written as:

$$s_i = \begin{cases} >0, & \text{if } i = 1, \cdots, P \\ 0, & \text{otherwise.} \end{cases} \tag{14}$$

In real scenarios, s_i is never exactly equaled to zero; however, it is very close to zero. In this case, the first solution is to define a false alarm probability like ε in the way that:

$$s_i = \begin{cases} >\varepsilon, & \text{if } i = 1, \cdots, P \\ <\varepsilon, & \text{otherwise.} \end{cases} \tag{15}$$

Nevertheless, it is still challenging to find a proper false alarm value. Motivated by Zhu et al. (2019), it is possible to define a new ratio-based method to avoid such a parameter selection problem. From Eq. (14), it is inferred that:

$$s_i = s_{i+1}, \quad \text{if} \quad i = P+1, \cdots, 77 \tag{16}$$

Consequently, a ratio-based criterion can be defined as:

$$r_i = \frac{s_{i+1}}{s_i} = 1, \quad \text{if} \quad i = P+1, \cdots, 77 \tag{17}$$

If a non-normalized design matrix is used, huge s values are obtained. Nevertheless, the r values for $i = P+1, \cdots, 77$ are still equal to one as expressed in Eq. (17). Practically, as shown in Fig. 1, the r values of a few last PCs, which have the lowest eigenvalues, are not equal to one. It is likely due to the high-level noise and errors in these PCs. It can also be due to the rounding errors in the computations. Although the r values of these PCs are not equal to one, these PCs are also considered

as the noise-related PCs. It is because we have already considered PCs with higher eigenvalues as noisy components, and so do we for the lower eigenvalues. Given the existence of these PCs, the final P value is determined as follows:

$$P = \max_j \left\{ j:\ r_i \neq 1,\ i = 1,\ \cdots, j \right\} \tag{18}$$

which completes our methodology on APCA-RFM.

3. Experiments

In this study, to evaluate the performance of the proposed method, we employed nine different data sets. They were acquired by different high resolution and medium resolution sensors. Detailed information of these data sets has been listed in Table 1. As shown in this table, the data sets are varied in terms of sensor type, region type, and spatial resolution.

The GCPs for the data sets have been provided by various techniques. In the L5-HJ and L5-L2 data sets, these points were extracted using geo-referenced images of the Landsat-5 satellite via automatic matching methods. For the PL-ISF, WV-ISF, Geo-ISF, IK-HMD, and Bum-IRS data sets, 1:2000 topographic maps were used to provide GCPs. The GCPs of S1A and S1B were obtained by a differential global positioning system (DGPS) method.

Three state-of-the-art methods, including L1LS (Long et al., 2015), USS-RFM (Alizadeh Moghaddam et al., 2018b), and PCA-RFM (Naeini et al., 2020), were applied as competing methods to comparatively analyze the performance of the proposed method in improving RFM optimization. The L1LS method attempts to excel RFM results by removing a number of unnecessary RPCs by imposing ℓ_1-norm of the RPCs to the main RFM problem. The USS-RFM method is also a method for eliminating additional RPCs based on Person correlation coefficient and significance testing, which has two single-stage and two-stage versions. As mentioned in Alizadeh Moghaddam et al. (2018b), the two-stage version yielded better results, hence, this version of USS-RFM has been used in the experiments. The PCA-RFM method, which is fully described in the previous sections and is the basis of the proposed APCA-RFM method, has been applied as another competing method.

In terms of tunable parameters, except for the proposed method, the other methods have indeed used such parameters. In the L1LS, there is a regularization parameter for the ℓ_1-norm term, which was set to $\lambda = 10^{-4}$ as stated in Long et al. (2015). The parameters of the USS-RFM method were also tuned as $\gamma = 10^{-6}$ and $\alpha = 0.2$ according to Alizadeh Moghaddam et al. (2018b). The PCA-RFM method also has a threshold parameter, set as $t = 10^{-2}$ as mentioned by Naeini et al. (2020).

The experiments, conducted in this study, have been divided into two main parts: 1) normal case analysis, and 2) limited number of GCPs analysis. In the first part, the performance of different methods was investigated on the experimental data sets with 40 and 50 GCPs. Moreover, in this part, the impact of the tunable threshold parameter on the PCA-RFM results was evaluated using 40 GCPs (i.e., when the degree of freedom is equal to one). In the second analysis, the potential of the different methods, when a limited number of GCPs is available, was investigated. In this experiment, different methods were implemented on the experimental data sets using 10, 15, 20, and 25 GCPs.

3.1. Normal case analysis

In this analysis, different methods have been implemented on the different data sets using 40 and 50 GCPs. For each case, the remaining GCPs have been used for the final evaluation of the methods. Obviously, in this analysis, S1A and S1B data sets are not useful because they include only 28 GCPs. To better examine different methods, five different data samples have been selected from the GCPs of the different data sets. Accordingly, each of the methods has been tested five times on each of these data sets. In each of these five tests, one of the data samples has been selected as training GCPs, and others have served as evaluating ones. Consequently, five RMSE values have been calculated for each data set that their average and standard deviation have been given as the final result.

Tables 2 and 3 show the results of the normal case analysis for the case of 40 and 50 GCPs, respectively. As can be seen, the L1LS method has had the weakest performance among the tested methods. The low accuracy (i.e., high RMSE value) of this method, especially in the L5-HJ, L5-L2, and IK-HMD data sets, is evident in these tables. However, in all cases in Tables 2 and 3, the standard deviation values are below 0.5 pixels, except for IK-HMD. The examination of these tables shows that the USS-RFM method has higher accuracies than the L1LS method according to the average RMSEs. This method has also reported standard deviation values below 0.6 pixels in all cases, except for Bum-IRS. The PCA-RFM and APCA-RFM methods generally had higher accuracies than the USS-RFM and L1LS methods. In both methods, sub-pixel average RMSEs have been reported in most cases (4 out of 7 cases when using 40 GCPs and 5 out of 7 when using 50 GCPs). With the standard deviation values less than 0.1 pixels in 4 cases (out of 7), when using 40 GCPs, and in 5 cases (out of 7), when using 50 GCPs, the results of the APCA-RFM method show its high stability. Analysis of the average performance in Tables 2 and 3 also shows that in the normal case, the APCA-RFM method was superior to the other methods in terms of both average and standard deviation of RMSEs. However, the results of PCA-RFM and APCA-RFM methods are close to each other. Under these conditions, the use of the statistical Mann–Whitney U test (Mann and Whitney, 1947) can help to clarify the differences between the results of these two methods.

To have an adequate size population for the Mann–Whitney U test, in a complementary experiment, we repeated PCA-RFM and APCA-RFM methods 100 times with various data samples. The results of the Mann–Whitney U test showed that, at the 95% confidence interval, the differences in RMSEs between the PCA-RFM and APCA-RFM methods were statistically significant. In other words, the statistical test showed that the slight improvement of APCA-RFM over PCA-RFM was statistically meaningful.

Table 1
Detailed information about the data sets used in this study.

Data Set	Satellite	GSD (m)	Area type	No. of GCPs
L5-HJ	HJ1	30	Plain	200
L5-L2	Landsat-5	30	Mountainous, Hilly	200
PL-ISF	Pleiades	0.5	Urban	70
WV-ISF	WorldView-3	0.5	Urban	70
IK-HMD	IKONOS	1	Urban	74
Geo-ISF	GeoEye-1	0.5	Urban	70
Bum-IRS	IRS-P5	2.5	Semiurban	77
S1A	Spot-3 1A	10	Rural, Mountainous	28
S1B	Spot-3 1B	10	Rural, Mountainous	28

Table 2
The average and standard deviation (Avg. ± Std. Dev.) of RMSEs (in pixel) obtained from the implementation of different methods on the five data samples of the experimental data sets using 40 GCPs.

Data set	L1LS	USS-RFM	PCA-RFM	APCA-RFM
L5-HJ	2.148 ± 0.223	0.853 ± 0.053	0.782 ± 0.160	0.778 ± 0.129
L5-L2	3.021 ± 0.313	1.371 ± 0.416	0.694 ± 0.046	0.711 ± 0.072
PL-ISF	1.039 ± 0.090	0.907 ± 0.066	1.055 ± 0.228	0.953 ± 0.166
WV-ISF	0.919 ± 0.170	0.908 ± 0.386	0.830 ± 0.128	0.902 ± 0.211
IK-HMD	3.550 ± 0.739	1.279 ± 0.055	1.215 ± 0.042	1.195 ± 0.064
Geo-ISF	1.082 ± 0.113	1.003 ± 0.104	0.844 ± 0.112	0.778 ± 0.075
Bum-IRS	1.570 ± 0.089	1.958 ± 1.524	1.547 ± 0.214	1.387 ± 0.069
Average	1.904 ± 0.248	1.183 ± 0.372	0.995 ± 0.133	0.958 ± 0.112

Table 3
The average and standard deviation (Avg. ± Std. Dev.) of RMSEs (in pixel) obtained from the implementation of different methods on the five data samples of the experimental data sets using 50 GCPs.

Data set	L1LS	USS-RFM	PCA-RFM	APCA-RFM
L5-HJ	2.184 ± 0.161	0.888 ± 0.014	0.752 ± 0.217	0.678 ± 0.071
L5-L2	3.040 ± 0.146	1.134 ± 0.513	0.655 ± 0.055	0.635 ± 0.026
PL-ISF	1.028 ± 0.138	0.793 ± 0.052	0.858 ± 0.063	0.817 ± 0.059
WV-ISF	0.786 ± 0.072	0.739 ± 0.056	0.753 ± 0.061	0.757 ± 0.049
IK-HMD	3.446 ± 0.629	1.299 ± 0.104	1.232 ± 0.082	1.226 ± 0.070
Geo-ISF	1.031 ± 0.142	0.965 ± 0.100	0.854 ± 0.283	0.793 ± 0.164
Bum-IRS	1.504 ± 0.082	2.279 ± 2.402	1.375 ± 0.200	1.358 ± 0.120
Average	1.860 ± 0.196	1.157 ± 0.463	0.926 ± 0.137	0.895 ± 0.091

To clarify the effect of the threshold parameter value in PCA-RFM, which was the primary motivation for the present study, we implemented the PCA-RFM method with different threshold values on the experimental data sets. In this analysis, 5 data samples with 40 GCPs were selected from each of the data sets. APCA-RFM results are also included in this part of the experiments. It is noteworthy that for the PCA-RFM with $t = 10^{-2}$ and the APCA-RFM methods, the results have already been presented in Table 2.

The results of this analysis are shown in Fig. 2. Evidently, in different data sets, the PCA-RFM method has reported different threshold values as the optimum one. For example, although $t = 10^{-1}$ had inferior results in the L5-L2 data set, it had the best performance in the PL-ISF and Bum-IRS data sets. PCA-RFM with $t = 10^{-3}$ had performed well in the L5-HJ and IK-HMD data sets; however, it had generally poor results. Moreover, $t = 10^{-4}$ generally yielded unacceptable results, even though, for the IK-HMD data set, the results for this threshold outperformed those for $t = 10^{-2}$, which has been suggested in Naeini et al. (2020). These examples show that the PCA-RFM method is sensitive to the threshold value, and it is almost impossible to provide a global threshold value. Conversely, considering the nature of the data, the APCA-RFM method is independent of the tedious operation of finding an appropriate threshold value and, on the other hand, has acceptable results in all data set tests. This is confirmed based on the results presented in Tables 2 and 3 and Fig. 2.

The computation cost is one of the crucial factors in the efficiency of an algorithm. All methods in our experiments were implemented on a personal computer having the Intel Core i5 CPU at 2.53 GHz and 5.80 GB usable RAM. It was observed that all methods run fast due to their simple mathematical implementations. Precisely speaking, per run, the average processing time of L1LS, USS-RFM, PCA-RFM, and APCA-RFM was 0.30, 0.12, 0.01, and 0.02 s, respectively. PCA-RFM and APCA-RFM are faster than the other two methods. APCA-RFM is slower than PCA-RFM by a factor of two due to its execution of an extra step to compute the threshold value. However, the methods investigated in the present contribution have no significant superiority in this regard as they all run fast enough.

Table 4
The average and standard deviation (Avg. ± Std. Dev.) of RMSEs (in pixel) obtained from the implementation of different methods on the five data samples of the experimental data sets using 10 GCPs. Asterisk indicates that the method has not converged to proper results in some data samples, and therefore, it has practically failed.

Dataset	L1LS	USS-RFM	PCA-RFM	APCA-RFM
L5-HJ	1.660 ± 0.197	0.874 ± 0.012*	1.525 ± 0.713	1.697 ± 0.610
L5-L2	2.284 ± 0.211	1.979 ± 0.286*	1.488 ± 1.220	1.549 ± 0.498
PL-ISF	0.990 ± 0.064	1.101 ± 0.013*	1.248 ± 0.188	1.295 ± 0.144
WV-ISF	0.886 ± 0.087	1.690 ± 0.222*	1.274 ± 0.447	1.225 ± 0.367
IK-HMD	3.131 ± 1.194	2.112 ± 0.121*	1.914 ± 0.629	1.384 ± 0.260
Geo-ISF	1.266 ± 0.201	1.251 ± 0.118	1.295 ± 0.438	1.267 ± 0.447
Bum-IRS	1.588 ± 0.437	1.690 ± 0.447*	1.822 ± 0.373	1.917 ± 0.320
S1A	3.606 ± 1.258	1.374 ± 0.230*	1.142 ± 0.277	1.594 ± 0.753
S1B	1.824 ± 0.543	1.081 ± 0.080*	1.145 ± 0.203	1.518 ± 0.412
Average	1.915 ± 0.466	1.461 ± 0.170*	1.428 ± 0.499	1.494 ± 0.423

Table 5
The average and standard deviation (Avg. ± Std. Dev.) of RMSEs (in pixel) obtained from the implementation of different methods on the five data samples of the experimental data sets using 15 GCPs. Asterisk indicates that the method has not converged to proper results in some data samples, and therefore, it has practically failed.

Dataset	L1LS	USS-RFM	PCA-RFM	APCA-RFM
L5-HJ	1.937 ± 0.246	0.938 ± 0.070	1.017 ± 0.112	1.034 ± 0.204
L5-L2	3.238 ± 0.681	2.292 ± 0.564*	1.133 ± 0.472	1.271 ± 0.552
PL-ISF	0.988 ± 0.081	0.906 ± 0.076	1.336 ± 0.324	1.077 ± 0.179
WV-ISF	0.896 ± 0.182	1.474 ± 1.201*	1.106 ± 0.155	1.130 ± 0.248
IK-HMD	2.938 ± 0.454	1.874 ± 0.301	1.517 ± 0.100	1.706 ± 0.274
Geo-ISF	1.048 ± 0.120	0.992 ± 0.034*	1.256 ± 0.249	1.002 ± 0.162
Bum-IRS	1.383 ± 0.158	4.237 ± 2.087*	2.338 ± 0.700	1.536 ± 0.083
S1A	2.605 ± 1.031	0.861 ± 0.120	0.909 ± 0.041	0.922 ± 0.075
S1B	1.406 ± 0.146	0.763 ± 0.098*	1.091 ± 0.293	1.122 ± 0.277
Average	1.827 ± 0.344	1.593 ± 0.506*	1.300 ± 0.272	1.200 ± 0.228

3.2. Limited number of GCPs analysis

This part of the experiments belongs to the examination of the behavior of different methods when a limited number of GCPs are available (i.e., the degree of freedom is negative). For this purpose, different methods were implemented on the experimental data sets using 10, 15, 20, and 25 GCPs. In each of these experiments, five data samples were

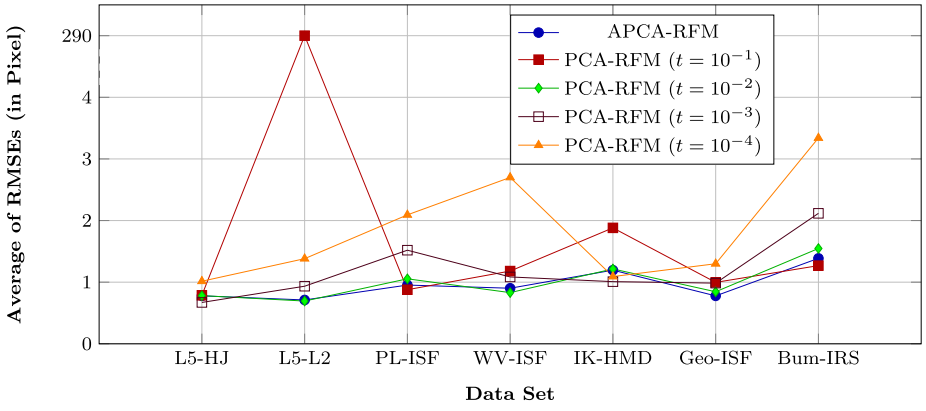

Fig. 2. Analyzing the effect of different threshold values in the results of PCA-RFM along with those of APCA-RFM.

Table 6
The average and standard deviation (Avg. ± Std. Dev.) of RMSEs (in pixel) obtained from the implementation of different methods on the five data samples of the experimental data sets using 20 GCPs. Asterisk indicates that the method has not converged to proper results in some data samples, and therefore, it has practically failed.

Dataset	L1LS	USS-RFM	PCA-RFM	APCA-RFM
L5-HJ	1.792 ± 0.118	0.838 ± 0.037	1.017 ± 0.140	1.091 ± 0.179
L5-L2	2.712 ± 0.465	1.185 ± 0.534	1.272 ± 1.175	1.283 ± 1.170
PL-ISF	0.927 ± 0.046	0.891 ± 0.076	1.242 ± 0.392	1.067 ± 0.076
WV-ISF	0.765 ± 0.034	0.960 ± 0.130	0.939 ± 0.129	0.922 ± 0.104
IK-HMD	2.791 ± 0.305	1.803 ± 0.124	1.724 ± 0.929	1.458 ± 0.304
Geo-ISF	1.018 ± 0.069	1.088 ± 0.154*	1.616 ± 1.380	0.925 ± 0.142
Bum-IRS	1.517 ± 0.136	1.502 ± 0.270	1.631 ± 0.169	1.350 ± 0.103
S1A	3.181 ± 0.694	0.740 ± 0.081	0.790 ± 0.119	0.822 ± 0.085
S1B	1.321 ± 0.247	0.816 ± 0.109	0.897 ± 0.107	0.945 ± 0.104
Average	1.780 ± 0.235	1.092 ± 0.168*	1.236 ± 0.504	1.096 ± 0.252

Table 7
The average and standard deviation (Avg. ± Std. Dev.) of RMSEs (in pixel) obtained from the implementation of different methods on the five data samples of the experimental data sets using 25 GCPs.

Dataset	L1LS	USS-RFM	PCA-RFM	APCA-RFM
L5-HJ	2.105 ± 0.398	0.953 ± 0.053	0.910 ± 0.209	0.868 ± 0.106
L5-L2	2.964 ± 0.220	0.867 ± 0.376	0.745 ± 0.077	1.009 ± 0.669
PL-ISF	1.068 ± 0.088	0.912 ± 0.090	0.973 ± 0.094	0.883 ± 0.060
WV-ISF	0.924 ± 0.110	0.860 ± 0.114	1.057 ± 0.215	1.007 ± 0.189
IK-HMD	3.446 ± 0.522	1.434 ± 0.095	1.451 ± 0.265	1.423 ± 0.271
Geo-ISF	1.045 ± 0.089	0.938 ± 0.076	1.475 ± 1.149	0.886 ± 0.114
Bum-IRS	1.407 ± 0.088	3.081 ± 2.566	1.554 ± 0.245	1.231 ± 0.041
S1A	2.832 ± 0.961	2.506 ± 2.816	0.770 ± 0.268	0.760 ± 0.216
S1B	1.541 ± 0.507	1.725 ± 2.208	0.753 ± 0.155	0.849 ± 0.244
Average	1.926 ± 0.331	1.475 ± 0.932	1.076 ± 0.297	0.990 ± 0.212

selected from each of the data sets. The average and standard deviation of the obtained RMSEs, from these five data samples, were reported as the final results for the comparison.

Tables 4–7 show the results of implementing different methods in the case of limited number of GCPs. In these tables, the results of the USS-RFM method are occasionally presented with asterisks. These asterisks indicate that the USS-RFM method has not converged to the proper results in some of the data samples of the corresponding data sets, or, in other words, the method has practically failed. In this case, the reported average and standard deviation values belong to the data samples that converged to acceptable results. In general, although the USS-RFM method had almost proper results with 25 GCPs, it can generally be stated that this method was unsuccessful when using a limited number of GCPs, especially in the case of 10 and 15 GCPs.

With 10 GCPs, the PCA-RFM and APCA-RFM methods generally outperformed the L1LS. In these methods, the average RMSEs were less than 2 pixels, whereas the averages RMSEs of the L1LS were 3.13 and 3.60 pixels in IK-HMD and S1A, respectively. In this experiment, the PCA-RFM method was partially better than the APCA-RFM method, although APCA-RFM's standard deviations were slightly less than those for PCA-RFM. Similar to the experiments with 10 GCPs, the PCA-RFM and APCA-RFM methods had better performance than the other two methods using 15 GCPs. Nevertheless, in this part, APCA-RFM outperformed PCA-RFM in both average and standard deviation values. Using 20 and 25 GCPs, the APCA-RFM had better performance than the other methods with less than 1.5-pixel average RMSEs in all data sets.

For a better presentation, the summation of total averages and standard deviations of RMSEs, given in the last rows of Tables 4–7, has been illustrated in Fig. 3. Because the USS-RFM failed in the experiments with 10, 15, and 20 GCPs, its results are not included in the corresponding graphs in this figure. As illustrated, APCA-RFM provides better results compared to other methods. Moreover, the accuracy of the results has consistently increased with increasing the number of GCPs.

The experiments in this part with limited number of GCPs also showed that, in general, the APCA-RFM method performed better than the competing ones. This superiority, as well as its independence of any tunable parameter, indicates the high efficiency of the APCA-RFM in determining RPCs.

4. Conclusions

In this study, to enhance the determination of RPCs, an automated method based on the PCA transformation and thresholding ridge ratio, called APCA-RFM, was presented to reduce the impact of noise and errors in the image and ground coordinates of GCPs, affecting the design matrix. In this method, which is an improved version of a

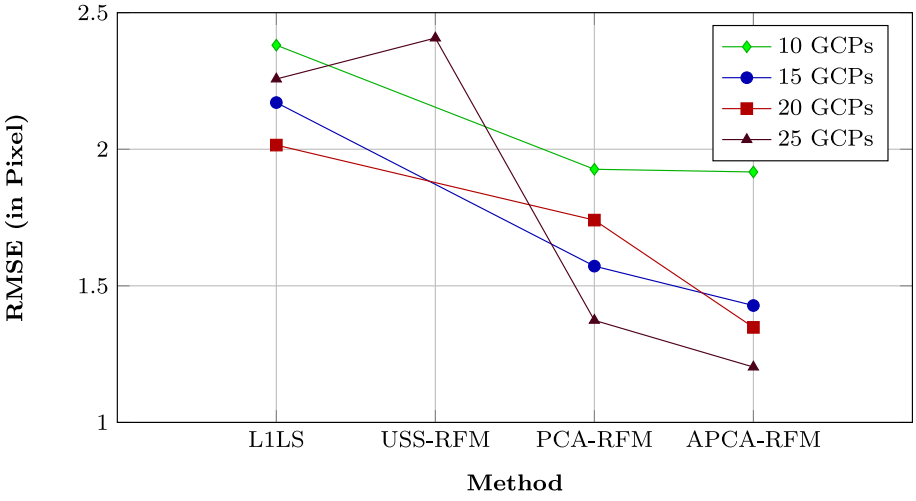

Fig. 3. The summation of total average and standard deviation of RMSEs, obtained from the implementation of different methods in the case of limited GCPs.

previously proposed PCA-RFM, first, the PCA transformation was performed on the design matrix. Therefore, 78 components, equal to the number of RPCs, were generated in the PC space. Some of these components are related to noise, and some others are signal components. The PCA-RFM method applies a pre-defined threshold value on the eigenvalues, corresponding to the PCs, to separate signal-related from noise-related PCs. However, in the APCA-RFM method, the number of signal-related PCs is automatically determined based on the thresholding ridge ratio criterion. After the removal of noise-related PCs, APCA-RFM performs an inverse PCA to achieve the noise-free design matrix. Such a design matrix is not ill-posed anymore, but strictly rank deficient.

The investigations in this study showed that the empirically tuned threshold value in the PCA-RFM method can significantly affect the final results. The results also revealed that this threshold value is case-study dependent. In contrast, considering the nature of the data, the APCA-RFM method separated the noise-related PCs from the signal-related ones in the PC space, avoiding the challenging problem of finding an appropriate threshold value. In addition, experiments conducted on different data sets using the proposed method along with USSRFM, L1LS, and PCA-RFM exhibited that the proposed method has higher accuracy and stability than other methods in determining RPCs.

This research focused on reducing the impact of noise on the ill-posed design matrix of the RFM problem. It is well known that some of the RPCs are unnecessary, and therefore, it is essential to remove the redundant ones, which leads to a well-posed design matrix. Accordingly, future studies will attempt to simultaneously reduce the noise and the number of RPCs to further increase the accuracy of the RPCs determination, and consequently, increase the geometric correction of the satellite images.

Declaration of Competing Interest

The authors declare that they have no known competing financial interests or personal relationships that could have appeared to influence the work reported in this paper.

Acknowledgements

The authors would like to thank Prof. M. J.Valadan Zoej, from K. N. Toosi University of Technology, Tehran, Iran, Dr. S. Homayouni from the Centre Eau Terre Environnement, INRS, Quebec, Canada, and Dr. S.B. Fatemi from the University of Isfahan, Isfahan, Iran for providing some data sets in our case studies. The authors also thank Dr. T. Long from the Chinese Academy of Sciences, Beijing, China, for sharing their python source code of L1LS and two experimental data sets, L5-HJ and L5-L2.

References

Alizadeh Moghaddam, S.H., Mokhtarzade, M., Alizadeh Moghaddam, S.A., 2018a. Optimization of rfm's structure based on pso algorithm and figure condition analysis. IEEE Geosci. Remote Sens. Lett. 15 (8), 1179–1183.
Alizadeh Moghaddam, S.H., Mokhtarzade, M., Alizadeh Naeini, A., Amiri-Simkooei, A., 2018b. A statistical variable selection solution for rfm ill-posedness and over-parameterization problems. IEEE Trans. Geosci. Remote Sens. 56 (7), 3990–4001.
Alizadeh Naeini, A., Alizadeh Moghaddam, S.H., Mirzadeh, S.M.J., Homayouni, S., Fatemi, S.B., 2017. Multiobjective genetic optimization of terrain-independent rfms for vhsr satellite images. IEEE Geosci. Remote Sens. Lett. 14 (8), 1368–1372.
Cao, J., Fu, J., 2018. Estimation of rational polynomial coefficients based on singular value decomposition. J. Appl. Remote Sens. 12 (4), 044003.
Chang, C.-I., Du, Q., 2004. Estimation of number of spectrally distinct signal sources in hyperspectral imagery. IEEE Trans. Geosci. Remote Sens. 42 (3), 608–619.
Gholinejad, S., Alizadeh Naeini, A., Amiri-Simkooei, A., 2019a. Robust particle swarm optimization of rfms for high-resolution satellite images based on k-fold cross-validation. IEEE J. Sel. Top. Appl. Earth Obser. Remote Sens. 12 (8), 2594–2599.
Gholinejad, S., Alizadeh Naeini, A., Amiri-Simkooei, A., 2019b. Handling ill-posedness and overparameterization of rational function model using bi-objective particle swarm optimization. Earth Obser. Geomatics Eng. 3 (1), 34–42.
Gholinejad, S., Naeini, A.A., Amiri-Simkooei, A., 2020. Discrete-binary configuration of metaheuristic algorithms for rfm optimization in the case of limited gcps. J. Appl. Remote Sens. 14 (2), 026508.
Golub, G.H., Van Loan, C.F., 2012. Matrix Computations, Vol. 3, JHU Press.
Jannati, M., Valadan Zoej, M.J., Mokhtarzade, M., 2017. A knowledge-based search strategy for optimally structuring the terrain dependent rational function models. Remote Sens. 9 (4), 345.
Long, T., Jiao, W., He, G., 2015. Rpc estimation via ℓ_1-norm-regularized least squares (l1ls). IEEE Trans. Geosci. Remote Sens. 53 (8), 4554–4567.
Mann, H.B., Whitney, D.R., 1947. On a test of whether one of two random variables is stochastically larger than the other. Annals Mathe. Stat. 50–60.
Moghaddam, S.A., Mokhtarzade, M., Naeini, A.A., Moghaddam, S., 2017. Statistical method to overcome overfitting issue in rational function models. Int. Arch. Photogramm. Remote Sens. Spatial Inf. Sci. 42, 1–4.
Naeini, A.A., Moghaddam, S.H.A., Sheikholeslami, M.M., Amiri-Simkooei, A., 2020. Application of pca analysis and qr decomposition to address rfm's ill-posedness. Photogramm. Eng. Remote Sens. 86 (1), 17–21.
Öztürk, F., Akdeniz, F., 2000. Ill-conditioning and multicollinearity. Linear Algebra Appl. 321 (1–3), 295–305.
Tao, C.V., Hu, Y., 2001. A comprehensive study of the rational function model for photogrammetric processing. Photogramm. Eng. Remote Sens. 67 (12), 1347–1358.
Tengfei, L., Weili, J., Guojin, H., 2014. Nested regression based optimal selection (nrbos) of rational polynomial coefficients. Photogramm., Eng. Remote Sens. 80 (3), 261–269.
Toutin, T., 2004. Geometric processing of remote sensing images: models, algorithms and methods. Int. J. Remote Sens. 25 (10), 1893–1924.
Valadan Zoej, M.J., Mokhtarzade, M., Mansourian, A., Ebadi, H., Sadeghian, S., 2007. Rational function optimization using genetic algorithms. Int. J. Appl. Earth Obs. Geoinf. 9 (4), 403–413.
Wu, Y., Ming, Y., 2016. A fast and robust method of calculating rfm parameters for satellite imagery. Remote Sens. Lett. 7 (12), 1112–1120.
Yuan, X., Lin, X., 2008. A method for solving rational polynomial coefficients based on ridge estimation. Geomatics Informat. Sci. Wuhan Univ. 33 (11), 1130–1133.
Zhang, Y., Lu, Y., Wang, L., Huang, X., 2012. A new approach on optimization of the rational function model of high-resolution satellite imagery. IEEE Trans. Geosci. Remote Sens. 50 (7), 2758–2764.
Zhou, Q., Jiao, W., Long, T., 2012. Solution to the rational function model based on the levenberg-marquardt algorithm. In: 2012 9th International Conference on Fuzzy Systems and Knowledge Discovery (FSKD). IEEE, pp. 2795–2799.
Zhu, X., Kang, Y., Liu, J., 2019. Estimation of the number of endmembers via thresholding ridge ratio criterion. IEEE Trans. Geosci. Remote Sens. 58 (1), 637–649.